Atomistic models of hydrogenated amorphous silicon nitride from first principles

K. Jarolimek,[1,2] R. A. de Groot,[2] G. A. de Wijs,[2] and M. Zeman[1]
[1]*PVMD/DIMES, Delft University of Technology, Feldmannweg 17, 2600 GB Delft, The Netherlands*
[2]*ESM, IMM, Radboud University Nijmegen, Heyendaalseweg 135, 6525 AJ Nijmegen, The Netherlands*
(Received 19 June 2010; revised manuscript received 22 September 2010; published 1 November 2010)

We present a theoretical study of hydrogenated amorphous silicon nitride (a-SiN_x:H), with equal concentrations of Si and N atoms ($x=1$), for two considerably different densities (2.0 and 3.0 g/cm^3). Densities and hydrogen concentration were chosen according to experimental data. Using first-principles molecular-dynamics within density-functional theory the models were generated by cooling from the liquid. Where both models have a short-range order resembling that of crystalline Si_3N_4 because of their different densities and hydrogen concentrations they show marked differences at longer length scales. The low-density nitride forms a percolating network of voids with the internal surfaces passivated by hydrogen. Although some voids are still present for the high-density nitride, this material has a much denser and uniform space filling. The structure factors reveal some tendency for the nonstoichiometric high-density nitride to phase separate into nitrogen rich and poor areas. For our slowest cooling rate (0.023 K/fs) we obtain models with a modest number of defect states, where the low (high) density nitride favors undercoordinated (overcoordinated) defects. Analysis of the structural defects and electronic density of states shows that there is no direct one-to-one correspondence between the structural defects and states in the gap. There are several structural defects that do not contribute to in-gap states and there are in-gap states that do only have little to no contributions from (atoms in) structural defects. Finally an estimation of the size and cooling rate effects on the amorphous network is reported.

DOI: 10.1103/PhysRevB.82.205201 PACS number(s): 61.43.Bn, 61.43.Dq, 71.23.Cq

I. INTRODUCTION

Hydrogenated amorphous silicon nitride (a-SiN_x:H) is a widely used dielectric material in the microelectronic industry. Its functions range from a passivation layer and selective etching mask to gate dielectric in thin-film transistors (TFTs).[1] Device applications include TFTs for liquid crystal displays,[2] nonvolatile semiconductor memory,[3] and a novel type of light-emitting diode.[4] The rapidly growing photovoltaic industry utilizes thin films of a-SiN_x:H to minimize reflection losses of solar cells.[5,6]

Thin films of silicon nitride are deposited using different types of chemical-vapor deposition (CVD) and sputtering.[7,8] The material is nonstoichiometric in general and contains considerable amounts of hydrogen depending on the preparation conditions.

Along with the experimental interest in a-SiN_x:H, several theoretical studies have been performed.[9–25] In general the studies consist of two consecutive parts. First one needs to obtain a structural model of the amorphous network. Next the electronic and vibrational properties can be analyzed. The preparation of structural models can be roughly divided into two approaches:

The first one is based on cooling from a liquid to room temperature. When the cooling rate is high enough, the system does not have time to crystallize and it ends up in a metastable (amorphous) state. The process of cooling is simulated either by molecular-dynamics (MD) or Monte Carlo calculations. The interaction between atoms can be described either by a force field (interatomic potentials) (Refs. 9–14) or with *ab initio* methods. The force-field calculations enable one to evolve relatively big systems for longer periods of time.[15–18] On the other hand the transition from liquid to solid poses difficult requirements on the interatomic potentials since the potential has to describe the liquid and solid phase accurately at the same time. In the case of silicon, for example, the coordination changes from ~6 to 4 and the system additionally undergoes a metal to semiconductor transition.[26] Quantum-mechanical calculations (mostly based on the density-functional theory [DFT]) provide a realistic description of the chemistry and bonding of the system but are restricted to smaller system sizes and shorter simulation times.[19–22]

The second approach to preparation of amorphous structures is based on an *a priori* assumption about a certain property of the network. We could, for example, require that all Si and N atoms are fourfold and threefold coordinated, respectively, or that the network is chemically ordered (there are no Si-Si and no N-N bonds). A classical example of such a method is the bond switching algorithm by Wooten *et al.*[23] applied to a-Si. It was recently extended by Kroll[24] to generate samples of a-Si_3N_4.[25] Ouyang and Ching[27] randomly combined six types of subunits to obtain a continuous random network model of a-Si_3N_4 with the correct topology.

A majority of the above studies are on pure stoichiometric silicon nitride. Calculations on hydrogenated material are more rare[14,24,25,28] and so far no entirely first-principles calculation has been performed. Depending on the plasma-enhanced CVD deposition conditions very different materials can be prepared: Giorgis *et al.*[7] deposited a material with density 2.0 g/cm^3 containing 30 at. % of hydrogen. A much more dense material is deposited when the feedstock gasses are diluted with hydrogen. This results in a material with density 3.0 g/cm^3 and 18 at. % of hydrogen.[7] Interestingly the hot-wire CVD technique also yields high-density films with a similar composition.[8]

In this study we investigate a-SiN_x:H with equal amounts of silicon and nitrogen ($x=1$). Our motivation is to understand the structure and electronic properties of nitrides other

than stoichiometric. We have prepared models for both low- and high-density phases of a-SiN:H utilizing the above-mentioned experimental compositions. The models of the amorphous network are prepared with the "cooling from liquid" method, that was successfully applied previously to study a-Si:H.[29,30] We analyze the short-range order and report on the coordination of atoms, the mean and deviation of the bond lengths. The possibility of void creation and phase separation at two very different densities is investigated. Defects, acting as trapping sites, can dramatically influence the transport properties of a material. We report both on Si- and N-based defects that are undercoordinated or overcoordinated. The electronic structure of the nitrides is analyzed. The character of the valence and conduction bands explains the relationship between the band-gap size and the nitride composition. The preparation of amorphous structures with the cooling from liquid method is arbitrary to some extend. Two major factors that affect the quality of the models are the cell size and the cooling rate used. We estimate these effects by comparing models prepared under different conditions.

The paper is organized as follows. Section II describes settings used during the calculations. The generation of the structural models is described in Sec III. Section IV contains three sections devoted to: structure at short range, structure at long range, defects and electronic properties. A discussion of the cell size and cooling rate effects is presented in Secs. V and VI. Our main findings are summarized in Sec. VII.

II. TECHNICAL DETAILS

The total energy and forces are calculated within DFT using the generalized gradient approximation.[31] All calculations were performed with the Vienna *ab initio* simulation package (VASP).[32,33] Electron-ion interactions are described using the projector augmented wave method.[34,35] MD calculations were performed with a "soft" nitrogen potential and a 250 eV kinetic-energy cutoff. For static calculations a 400 eV cutoff and "normal" potentials supplied with VASP were used. The performance of the potentials was tested on α and β phases of Si_3N_4. The calculated cell parameters were higher than experimental ones by less than 1%. The difference in cell parameters between the soft and normal potential was less than 0.1%. During the whole MD run and the relaxation, we use only the Γ point for Brillouin-zone sampling. When calculating the density of states (DOS) of the relaxed structures the Brillouin zone is sampled with a $3\times3\times3$ and a $5\times5\times5$ Monkhorst-Pack mesh[36] for the "big" and "small" cells (for an explanation, see below), respectively. In both cases a Gaussian smearing with a width of 0.05 eV is used. Molecular-dynamics calculations were performed with a 1 fs time step.

III. PREPARATION OF THE STRUCTURE

The amorphous structures are prepared by the cooling from liquid approach. At first atoms are placed randomly in the supercell at distances larger than the sum of their covalent radii. This prevents large forces at the start of the MD calculation. The velocities of the atoms are initialized according to the Maxwell-Boltzmann distribution such that the temperature of the system is 300 K. Next the system is heated to 3060 K with a constant rate of 1.38 K/fs. The temperature is controlled by velocity rescaling at each MD step. At 3060 K the system is a liquid with the root mean squared displacement growing linearly in time. The density of states has a depression around the Fermi energy, however no band gap is formed. The liquid is equilibrated for 8 ps at this temperature. Next the sample is cooled back to room temperature. We utilize two different cooling rates: 1.380 and 0.023 K/fs (see Fig. 1). We will refer to them as the fast and the slow cooling rate. After reaching 300 K the samples are evolved for another 0.5 ps to calculate the structural averages. Next the structures are relaxed in order to calculate the electronic properties.

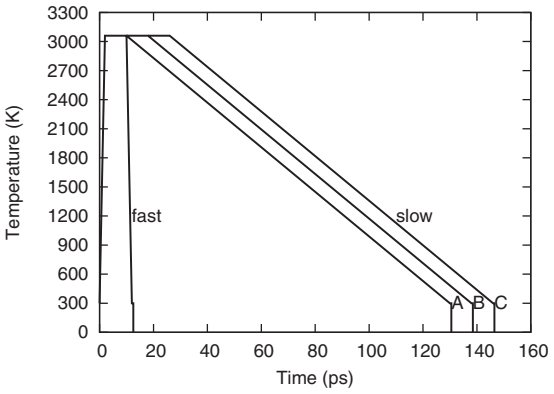

FIG. 1. Thermal procedure used to prepare amorphous structures of a-SiN:H The three slow quench samples are marked with letters A, B, and C.

The low-density cell $Si_{128}N_{128}H_{114}$ is cubic with a side of 16.59 Å. The high-density cell $Si_{194}N_{194}H_{85}$, containing much less hydrogen, has the same dimensions. Both were prepared with the slow cooling rate and we will refer to them as big cells. Additionally, we have prepared four small cells $Si_{38}N_{38}H_{34}$ with dimensions 11.06 Å $\times$ 11.06 Å $\times$ 11.09 Å. These cells contain low-density nitride. One was prepared with the fast cooling rate and three with the slow cooling rate. The compositions and densities are based on measurements by Giorgis *et al.*[7] Unless stated otherwise, below we report data on the big cells only.

IV. LOW- AND HIGH-DENSITY PHASES OF a-SiN:H

A. Structure at short range

Although amorphous silicon nitride lacks the long-range order of a crystal, the strong covalent bonding orders the atoms at shorter distances. This short-range order is to some extent similar to the crystalline α and β stoichiometric phases, where Si atoms are bonded to 4 N atoms with bonds defining a tetrahedral angle of 109° and N atoms bonded to 3 Si atoms in a planar configuration with angles of 120°. Indeed the bond angle distributions of a-Si_3N_4 reported by Giacomazzi and Umari have means close to the above values.[22] The distributions are however considerably broadened. Since

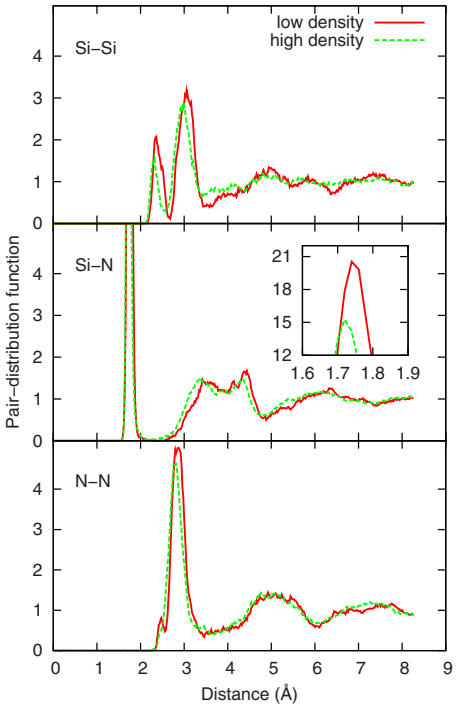

FIG. 2. (Color online) Partial pair distributions of big cells: Si-Si (upper part), Si-N (middle part), and N-N (lower part). The red solid and green dashed lines correspond to the low- and high-density nitride, respectively. All curves refer to systems at 300 K.

the material under study is silicon rich and contains a considerable amount of hydrogen there are also differences.

In order to characterize the short-range order in amorphous solids pair-distribution functions $g(r)$ are routinely employed. These give the probability of finding two atoms at a distance r apart in the system under study, normalized by this probability for a completely disordered system at the same density. Since our samples contain three different chemical elements there is a total of six partial distributions. In Fig. 2 we plot only partial distributions that do not contain hydrogen. In both the low- and high-density phases the Si-Si pair distribution has two prominent peaks. The first peak gives a hint that the material is nonstoichiometric. It is mostly due to Si-Si bonds but also contains a small contribution from silicon atoms that form square-shaped structures. These "square structures" are formed by two silicon atoms in opposite corners of a square along with two nitrogen atoms placed in the remaining corners. The structure is planar with angles close to 90°. Similar structures were observed before in theoretical models of a-Si_3N_4. Kroll reports on four-membered rings that induce peaks at 90° in the bond-angle distributions.[24] Giacomazzi and Umari[22] describe the very same structure as "edge-sharing tetrahedra." The second peak in g_{SiSi} is formed by silicon atoms that are connected to a common nitrogen atom. The first peak of g_{NN} has a shoulder due to nitrogen atoms that form the square structures. Nitrogen atoms bonded to a common silicon atom contribute to the first main peak. Note that there are no N-N bonds present in the samples and thus the corresponding peak is missing. The Si-H and N-H pair distributions (not shown) have well-defined and sharp first peaks that are due to hydrogen bonded to silicon or nitrogen atoms, respectively. The peak positions in g_{SiH} and g_{HN} correspond to calculated bond lengths in the SiH_4 and NH_3 molecules, respectively. A similar amount of hydrogen molecules is formed in both samples: 16 and 10 for low- and high-density nitride, respectively.[37]

Examining the structure of the low-density nitride, we find that it has a very open structure with void space that forms a percolating network. The internal surface of the voidlike structure accommodates most of the hydrogen who bind to Si and N. The H_2 molecules reside in the void space. The high-density nitride contains 1.5 times more Si and N atoms in the same volume and thus has a much higher packing. We note that both crystalline phases have a density of 3.2 $\mathrm{g/cm^3}$,[38] comparable to the density of our high-density material. Additionally to void space being filled up we find structural changes in the network.

As can be seen in Fig. 2 all peaks in the pair distributions have a smaller intensity in the high-density nitride, indicating that it is more disordered. As a general trend we find that bonds in the high-density nitride are compressed as compared to the low-density phase (see Table I). The first peak in the g_{SiSi} distribution shifts from 2.41 to 2.35 Å. The silicon-nitrogen bonds are more rigid and their length changes by only 0.01 Å. The second neighbor distances in the g_{SiSi} and g_{NN} shift to smaller distances as well. This implies that the average angles centered at the nitrogen and silicon atoms, respectively, are smaller in the high-density nitride. The change in the geometry of the square structures is small. The Si-Si and the N-N distances are compressed by 0.01 Å and 0.02 Å, respectively, in the dense nitride. Surprisingly, in the cell with a higher atomic density there are only eight square

TABLE I. Peak position r and width σ (or standard deviation of the distance) in pair-distribution functions not containing hydrogen. Superscripts indicate either the first or second peak. All values were obtained from relaxed structures and thus refer to systems at 0 K. Values are in angstrom.

Cell	$r^1_{\mathrm{Si\text{-}Si}}$	$r^2_{\mathrm{Si\text{-}Si}}$	$r^1_{\mathrm{Si\text{-}N}}$	$r^1_{\mathrm{N\text{-}N}}$	$\sigma^1_{\mathrm{Si\text{-}Si}}$	$\sigma^2_{\mathrm{Si\text{-}Si}}$	$\sigma^1_{\mathrm{Si\text{-}N}}$	$\sigma^1_{\mathrm{N\text{-}N}}$
Fast	2.410	3.084	1.753	2.904	0.071	0.178	0.050	0.143
Slow A	2.449	3.080	1.765	2.912	0.097	0.161	0.033	0.144
Slow B	2.415	3.081	1.756	2.913	0.089	0.162	0.029	0.142
Slow C	2.416	3.038	1.758	2.924	0.066	0.145	0.032	0.145
Low dens.	2.414	3.087	1.758	2.917	0.081	0.160	0.035	0.155
High dens.	2.352	3.030	1.745	2.854	0.079	0.184	0.045	0.152

TABLE II. Coordination of silicon and nitrogen atoms in the low- and high-density nitride. Artificial Si-Si bonds are discarded from the count.

	Si by Si	Si by N	Si by H	Si by all
Low dens.	0.84	2.68	0.45	3.98
High dens.	0.88	2.90	0.26	4.04
	N by Si	N by N	N by H	N by all
Low dens.	2.68		0.30	2.98
High dens.	2.90		0.13	3.03

structures compared to the low-density cell which contains 14 of the structures. The fluctuation in these values could be deduced from the small cells, where the deviation in the number of square structures is around 1 (see Table III). It is not expected that the structures are remnants of the liquid phase because their concentration is lower at higher temperatures.

In order to calculate coordination numbers, six cut-off distances need to be defined. The cut-off distances are chosen as the position of the minimum after the first peak in the corresponding partial pair distribution. The exception to this rule is the N-N bond since there are no such bonds present in our samples. The N-N cut-off distance is set approximately to the bond length of the N_2 molecule (1.20 Å). The minima in the Si-Si pair distribution are different for the two samples. Hence we use also different cut-off distances for low- and high-density nitride (2.65 Å and 2.55 Å, respectively). For the Si-N pair a cut-off distance of 2.00 Å is used. The Si-H and N-H cut-off distances are 1.65 Å and 1.15 Å, respectively. Two H atoms are considered bonded when less than 0.85 Å apart.

In Table II the coordination distributions of the low- and high-density nitride are listed. As expected, in both the low- and the high-density system the number of first neighbor is close to what is ideally expected, given the valence of the atoms: 3.98 and 4.04 for Si (low- and high-density nitride, respectively) and 2.98 and 3.03, respectively. So there seems to be slight tendency for undercoordination (overcoordination) in the low (high) density nitride. The ratio of Si-H bonds to N-H bonds is 1.53 and 2.00 for the low- and high-density nitride, respectively. Thus hydrogen atoms form bonds preferably to silicon at both densities.

B. Structure at longer length scales

To analyze the structure at intermediate and longer length scales and study how it copes with nonstoichiometry we discuss the structure factors that provide a more natural means. The Ashcroft-Langreth[39] (AL) and Bhatia-Thornton[40] (BT) structure factors are plotted in Figs. 3 and 4, respectively. Both sets of structure factors have been constructed only from silicon and nitrogen atoms, disregarding any hydrogen contributions. The partial structure factors $S_{nn}(q)$, $S_{nc}(q)$, and $S_{cc}(q)$ are Fourier transforms of the (real-space) pair-distribution functions that describe correlations among number density and concentration fluctuations. A direct comparison with experiment is possible through the neutron structure factor in Fig. 5. Here the hydrogen atoms were included in the calculation. We have used scattering lengths of 4.1491 fm, 9.36 fm, and −3.739 fm for silicon, nitrogen, and hydrogen, respectively.[41]

In both the high- and the low-density nitride the S_{cc} has a pronounced main peak at $q \approx 2.8$ Å^{-1}. This corresponds to a real-space distance of roughly $7.7/2.8=2.8$ Å, which is close to the position of the main peak of g_{NN} (2.9 Å)and only slightly further from the main peak in g_{SiSi} (3.0–3.1 Å). Indeed it signals the concentration fluctuations that occur because of the main structural motif: the Si-N-Si and N-Si-N with quite rigid bond angles giving rise to homocoordination at the corresponding length scale. The main peak in S_{nn} occurs just below 5 Å^{-1}, roughly corresponding with a real-space distance of 1.6 Å, quite close to the peak in g_{SiN} (1.75 Å).

In the following we focus on the differences between the high- and low-density nitride. In the high-density nitride a "prepeak" in S_{nn} occurs almost at the same q as the main peak in S_{cc}, i.e., around $q=2.5$ Å^{-1}. The peak in S_{nn}, however, is much broader than the sharp peak in S_{cc}. Moreover, it is shifted toward smaller wave vectors. Evidently the number density fluctuations occur at slightly longer and less sharply defined distances as the concentration fluctuations. This peak coincides with a similarly shaped peak in S_{SiSi} suggesting that it originates from fluctuations in the Si number density. These fluctuations might be a way how the system tries to cope with the nonstoichiometry but such a conclusion re-

TABLE III. A summary of defects present in different samples. Artificial Si-Si bonds inside square structures are discarded from the count. The number of the structures is listed in the first column. S2 denotes a twofold-coordinated silicon atom. Column denoted by D_{str} contains total counts of structural defects. Column D_{elc} gives the integrated DOS inside the band gap. The last column contains cohesive energies of cells per Si atom in electron volt.

Cell	Sq	Si2	Si3	Si5	H0	N2	N4	D_{str}	D_{elc}	E_{coh}
Fast	5	0	5	2	0	2	1	10	12	17.91
Slow A	4	0	0	0	0	1	1	2	4	18.17
Slow B	5	0	0	0	0	0	0	0	0	18.24
Slow C	6	0	1	0	0	1	0	2	2	18.19
Low dens.	14	1	4	3	2	3	0	13	12	18.21
High dens.	8	0	5	11	0	0	6	22	14	

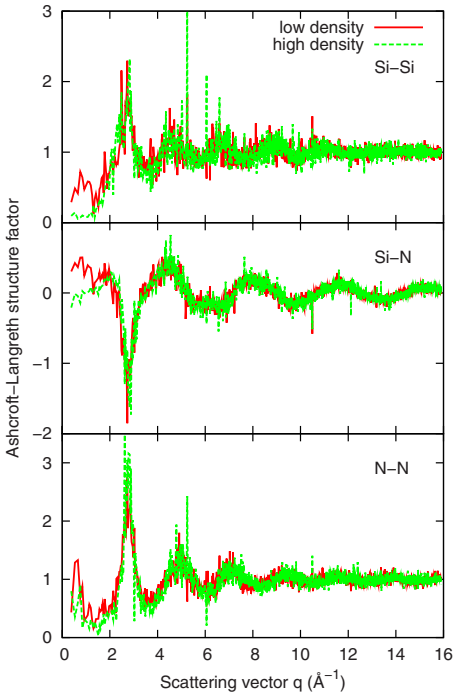

FIG. 3. (Color online) Calculated Ashcroft-Langreth structure factors of the low-density (red solid line) and high-density (green dashed line) nitride. Structure factors are averages over 500 MD steps (at 300 K) and were calculated for the big cells.

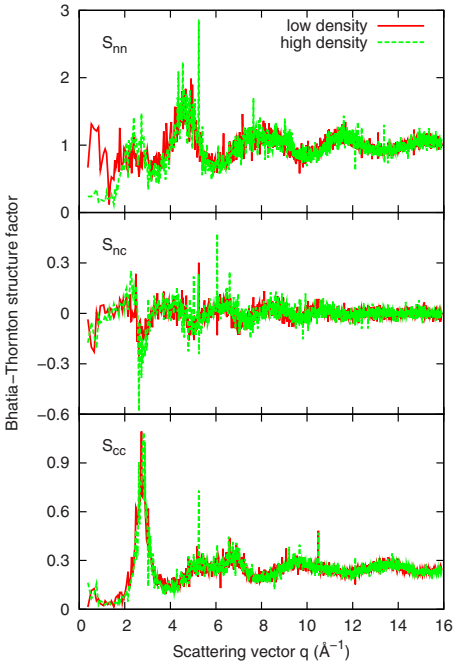

FIG. 4. (Color online) Calculated Bhatia-Thornton structure factors of the low-density (red solid line) and high-density (green dashed line) nitride. Structure factors are averages over 500 MD steps (at 300 K) and were calculated for the big cells.

mains speculative. Indeed we do not know the S_{cc} of the stoichiometric silicon nitride, but its neutron structure factor has a small hump at $q \approx 2.0$ Å^{-1}, just before the large peak at $q=2.8$ Å^{-1}.[42] At the longest wavelengths that we can access in our small cells, we observe a considerable increase in S_{NN} again, but not in S_{SiSi}. Evidently the dense nitride tries to deal with the nonstoichiometry by creating nitrogen-rich and nitrogen-poor regions, showing some tendency to phase separation. Concomitantly the S_{cc} shows a small upward bend for $q \to 0$.

Now let us consider the low-density nitride. Where in the high-density nitride only S_{NN} shows an appreciable increase for $q \to 0$, here all three AL partials have considerable values in this limit. Turning toward the BT structure factors, we see this translated in all of them. S_{cc} is very similar to the high density S_{cc} over the whole q range in Fig. 4. In the low-q range it has a small peak near 0.6 Å^{-1} that signals large scale composition fluctuations. On the other hand there is a downturn for the minimal q value that prevents an unambiguous conclusion about the phase separation. Additionally, the statistical noise is large for these small q values. The most striking effect is observed for S_{nn}. For large q values it traces the high density S_{nn} rather closely, but it does not have a prepeak near $q=2.5$ Å^{-1}, and moreover retains a large amplitude for all q in the long-wavelength limit. This is a clear signature of the void formation, which exposes a large internal surface area that is covered with saturating hydrogen atoms. Thus, for the low-density nitride, we observe long-wavelength composition fluctuations, but more importantly, we also see density fluctuations coming from the void formation.

C. Defects and electronic properties

The notion of a defect in an amorphous solid is linked to the coordination of an atom. Atoms that deviate from the proper coordination (Si fourfold, N threefold, and H onefold) are considered to be defects. Previously we have defined cut-off distances that enable us to retrieve the coordination of an atom. It turns out, however, that here the cut-off criterion is a too simple one: The two silicon atoms making up the "square structure" are within the specified cut-off distance but are not bonded. These "bonds" are artificial and we account for this fact in the coordination and defect counts.

In Table III we give an overview of defects found in the low- and high-density nitride samples. In absolute values

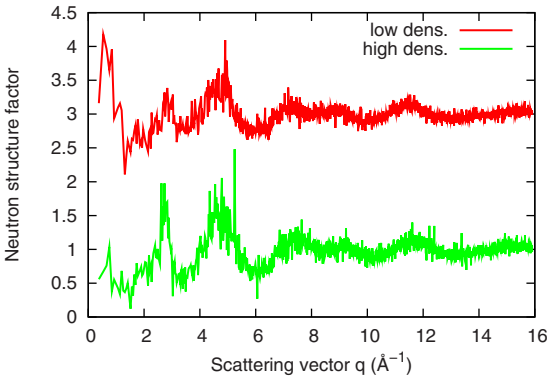

FIG. 5. (Color online) Calculated neutron structure factors of the low-density (red solid line) and high-density (green dashed line) nitride. Structure factors are averages over 500 MD steps (at 300 K) and were calculated for the big cells.

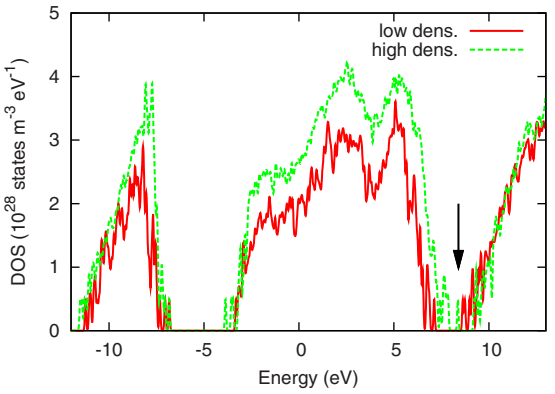

FIG. 6. (Color online) Calculated electronic density of states of the low-density (red solid line) and high-density (green dashed line) nitride. Both curves are aligned with respect to the center of mass of occupied states (at 0 eV). The arrow marks the Fermi energy of both cells.

there are more defects in the high-density nitride. When taking the number density into account the defect concentrations are similar. Interestingly there are 2.6 times more Si defects than N defects at both densities. The low-density nitride favors undercoordinated defects, whereas the high-density material favors overcoordinated defects.

In Fig. 6 we show the calculated electronic density of states of the big cells. The DOS curves are aligned at the "center of mass" of occupied states. We find that throughout the low-density cells the overall shape of the valence band, represented by the center of mass of occupied states, is similar. The variations are larger in the gap region. This method is thus more robust than aligning at the top of the valence band and will be used in the following discussion. From Fig. 6 we see that both models have a clearly defined band gap. The low-density nitride has a gap of 2.2 eV. The band gap of the high-density nitride is larger by 0.5 eV at a range of DOS levels. Note, that DFT underestimates semiconductor band gaps in general.

Next we calculate the site projected DOS, which enables us to split the total DOS into contributions from different chemical elements (see Fig. 7). We find that in the case of amorphous silicon nitride, the edges of the valence band extending from −3 to 7 eV are dominated by states localized at silicon atoms. The middle part of the band originates mostly from states located at nitrogen atoms. In the crystalline phases, that are stoichiometric, the situation is different. The lower part of the band is due to silicon and the upper part due to nitrogen. The conduction band is formed by silicon states in both cases. This finding is in agreement with measurements of the optical gap with varying composition of a-SiN_x:H. The band gap increases with increasing nitrogen content or decreasing number of Si-Si bonds.[7,43]

All of the samples except sample B contain a number of in-gap electronic defect states. In the following we will compare the amount of structural and electronic defects using two approaches. In the first approach, we integrate the density of states inside the gap. The range of integration (band-gap edges) depends on the density and is indicated in Fig. 8. In the low-density nitride the amount of defect states ob-

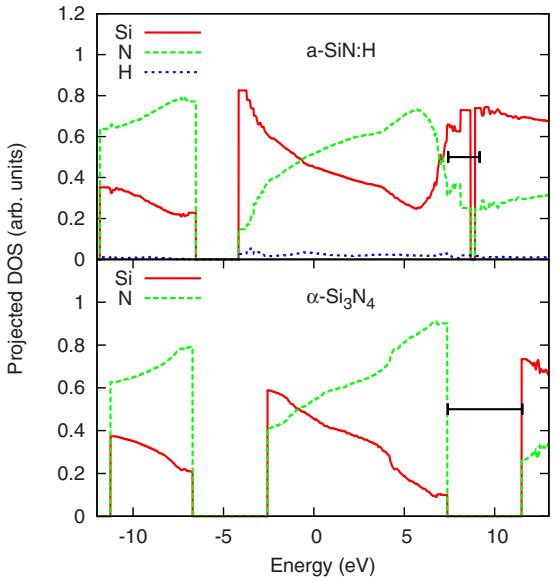

FIG. 7. (Color online) Relative contribution of silicon (red solid line), nitrogen (green dashed line), and hydrogen (blue dotted line) atoms to the total DOS. The case of high-density nitride and α-Si_3N_4 is shown in the top and bottom panel, respectively. Horizontal bars mark the band-gap region. All curves are aligned with respect to the center of mass of occupied states (at 0 eV).

tained in this way is comparable with the number of structural defects (see Table III). The agreement is worse for the dense nitride. In the second approach, we again make use of the site-projected DOS. This time, however, we sum over atoms that are structural defects. As can be seen from Fig. 8

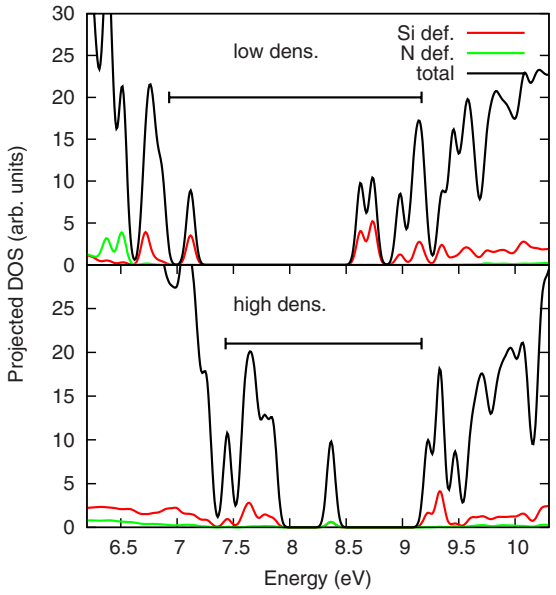

FIG. 8. (Color online) Density of states due to structural defects of the low (top panel) and high (bottom panel) density nitride. Contributions from silicon and nitrogen defect atoms are shown in red and green, respectively. The total projected DOS, summed over all atoms, is in black. The horizontal bars mark the band gaps. All curves are aligned with respect to the center of mass of occupied states (at 0 eV).

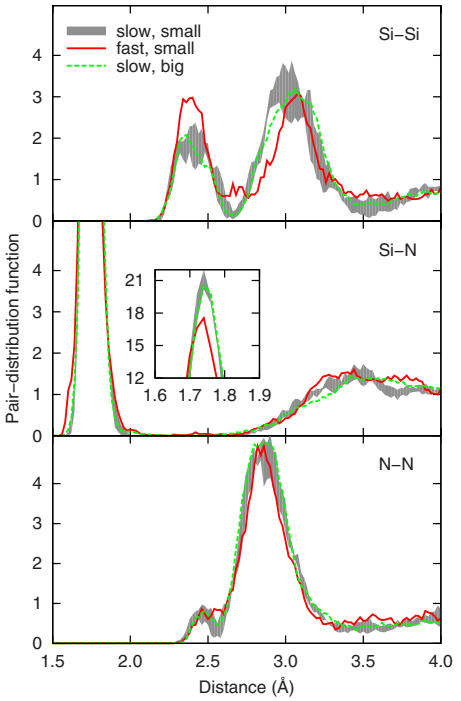

FIG. 9. (Color online) Comparison of pair distributions of the small cells prepared by slow cooling (gray), small cell prepared by fast cooling (red solid line), and the big low-density cell prepared by slow cooling (green dashed line). The gray area extends from the minimum to the maximum values determined from the distributions of samples A, B, and C. Only partial distributions not containing hydrogen are shown: Si-Si (upper part), Si-N (middle part), and N-N (lower part). All curves refer to systems at 300 K.

the major contribution to in-gap states comes from silicon atoms. Note, that the sum over the structural defects does not add up to the total DOS inside the gap regions. From this follows that the in-gap states have contributions from nondefective atoms. Additionally, there are structural defects that do not contribute to in-gap states. The ratio of electronically active defects is one half in the small cells and decreases to one third in big cells. Thus, in our models, we do not observe a one-to-one correspondence between structural and electronic defects.

V. CELL SIZE EFFECTS

First-principles methods, being more computationally intensive, are restricted to smaller system sizes. Here we investigate how the properties of the amorphous network change when comparing the small and big cells prepared with the slow cooling rate. Only cells containing low-density nitride are used for this purpose.

As can be seen in Fig. 9 there are no statistically significant effects on the pair distributions by the cell size. The peak positions and widths are similar in the small and big cells. The biggest discrepancy is in the second peak of g_{SiSi}, which for the small cells is shifted to lower values by 0.02 Å (see Table I). For both cell sizes the silicon atoms show a tendency to undercoordination. There are also more undercoordinated than overcoordinated defects. The same trend holds for nitrogen atoms with an average undercoordination and more undercoordinated defective nitrogen. The ratio of Si-H to N-H bonds is 1.41 and 1.53 for the small and big cells, respectively. The cohesive energies per Si atom are similar for different cell sizes (see Table III). The only parameter that stands out in the comparison is the number of defects (see Table III). If we would merge the three small samples they would have four defects out of 330 atoms. The big cell, containing 13 defects out of 370 atoms, has quite a higher defect concentration. A possible explanation for this behavior would be that bigger cells, having more degrees of freedom, result in an increased defect formation.

VI. COOLING RATE EFFECTS

The preparation of models of amorphous solids by cooling from the liquid is arbitrary to some extent. It does not mimic the experimental process. Cooling rates that are too high will result in structures with an excess of disorder. In previous studies, Alvarez *et al.*[20,21] quenched samples that were heated just below the melting temperature with a rate of 3.1 K/fs. Giacomazzi *et al.*[22] cooled their sample from 3500 to 2000 K, using a rate of 0.3 K/fs. Both authors studied pure silicon nitride. In this section we attempt to asses the effect of the cooling rate on the amorphous network.

Figure 9 shows the comparison of the small cells prepared by fast and slow cooling rate. The biggest effects are again in the Si-Si partial distribution. The positions of the first and second peak do not change significantly. The disorder in the "fast" cell is rather manifested by larger variations in the second-neighbor distances (0.178 Å for the Si-Si pair), that are proportional to deviations in bond angles. The number of square structures is comparable, however there are much more Si-Si bonds in the sample prepared by the fast rate. The faster cooling rate also seems to result in more variation in the Si-N bond length. After a fast quench the cell contains a large number of hydrogen molecules and defective threefold-coordinated silicon atoms. When using a slower cooling the hydrogen gets incorporated into the network more effectively, passivating undercoordinated defects. The bonding of hydrogen to nitrogen is mostly unaffected.

As mentioned above a sizable difference between the cells is the number of defects they contain. With the use of the slow cooling rate, we were in fact able to prepare a defect-free structure (sample B). Cells containing hundreds of atoms should be defect free in order to be comparable with the real device quality material. In the past, with very short simulation times, this has however proven to be difficult to achieve. Table III summarizes the number of defects for different cooling rates discarding any artificial bonds from the count. The fast quench cell, being more disordered has also the lowest cohesive energy among all the slow quench cells (see Table III).

VII. CONCLUSIONS

Atomistic models of a-SiN:H with equal amounts of silicon and nitrogen were prepared for two very different densities; 2.0 and 3.0 $\mathrm{g/cm^3}$. The short-range order is to some

extent similar to the crystalline α and β stoichiometric phases. Silicon atoms are mostly fourfold coordinated forming a tetrahedral unit. Nitrogen atoms are mostly threefold coordinated with bonds lying in a plane. Since the material under study is silicon rich and contains a considerable amount of hydrogen there are also differences. We find Si-Si bonds (but no N-N bonds). There are square structures consisting of two Si and two N atoms positioned in opposite corners of a square. The low-density nitride has a very open structure with void space that is largely connected into a percolating network. The internal surface accommodates the covalently attached hydrogen. When the density is increased this void space is filled up. Moreover, bonds get compressed, bond angles get smaller and the average coordination increases. At both densities the ratio of Si-H to N-H bonds is larger than 4/3 indicating the preference of hydrogen to bind to silicon.

Interestingly, the analysis of the structure at longer range revealed some tendency for the high-density nitride to phase separate. The Bhatia-Thornton structure factors show that nitrogen rich and nitrogen poor regions are formed (this is very hard to see just from plots of the three-dimensional structure, as only few atoms are involved). In the low-density nitride long-wavelength composition fluctuations also occur but a tendency to phase segregation is less evident. In contrast with the high-density material, here we observe the formation of void space, that is confirmed by the calculated structure factors. We note that the low-density nitride has a 1.5 times smaller density and a $\sim$1.3 times higher hydrogen concentration compared to the dense nitride.

In the second part of the paper we investigate coordination defects and electronic properties of a-SiN:H. We find that at both densities there are more Si defects than N defects. The high-density phase has a higher defect concentration because of the higher number density. The high-density nitride favors overcoordinated defects while the low-density phase favors undercoordinated defects. We have calculated the density of states for both phases and find a DFT gap of 2.2 eV and 1.7 eV for the low- and high-density nitride, respectively. The density of states at the band gap edges is dominated by states localized at silicon atoms. Decreasing silicon content opens up the gap, which is consistent with experimental knowledge. We find that less than half of the structural defects are electronically active. In the low-density nitride, integrating the DOS in the gap region gives values close to the number of structural defects. This approach is not universal and fails for the dense nitride.

In the final part of the paper we investigate whether the small cell systems are more affected by the constraints by the periodic boundary conditions, but we do not find any statistically significant differences, except for the number of defect states. We also try to estimate the effect of the cooling rate on the amorphous network. The samples prepared by fast cooling seem to be more disordered, with larger bond angle deviations, more defects and a higher cohesive energy. Using a rate of $\sim$0.02 K/fs we succeeded in preparing a defect-free structure containing $\sim$100 atoms.

ACKNOWLEDGMENTS

This work was carried out with a subsidy of the Dutch Ministry of Economic Affairs under EOS-LT program (Project No. EOSLT02028) and is a part of the research program of the Stichting voor Fundamenteel Onderzoek der Materie (FOM). FOM is financially supported by the Nederlandse Organisatie voor Wetenschappelijk Onderzoek (NWO).

[1] D. R. Cote, S. V. Nguyen, A. K. Stamper, D. S. Armbrust, D. Többen, R. A. Conti, and G. Y. Lee, IBM J. Res. Dev. **43**, 5 (1999).
[2] Y. Kuo, Vacuum **51**, 741 (1998).
[3] J. Bu and M. H. White, Solid-State Electron. **45**, 113 (2001).
[4] N. M. Park, C. J. Choi, T. Y. Seong, and S. J. Park, Phys. Rev. Lett. **86**, 1355 (2001).
[5] A. G. Aberle, Sol. Energy Mater. Sol. Cells **65**, 239 (2001).
[6] A. Elamrani, I. Menous, L. Mahiou, R. Tadjine, A. Touati, and A. Lefgoum, Renewable Energy **33**, 2289 (2008).
[7] F. Giorgis, C. F. Pirri, and E. Tresso, Thin Solid Films **307**, 298 (1997).
[8] R. E. I. Schropp, S. Nishizaki, Z. S. Houweling, V. Verlaan, C. H. M. der Werf, and H. Matsumura, Solid-State Electron. **52**, 427 (2008).
[9] P. Vashishta, R. K. Kalia, and I. Ebbsjö, Phys. Rev. Lett. **75**, 858 (1995).
[10] N. Umesaki, N. Hirosaki, and K. Hirao, J. Non-Cryst. Solids **150**, 120 (1992).
[11] F. de Brito Mota, J. F. Justo, and A. Fazzio, Phys. Rev. B **58**, 8323 (1998).
[12] F. De Brito Mota, J. F. Justo, and A. Fazzio, Int. J. Quantum Chem. **70**, 973 (1998).
[13] K. Matsunaga and Y. Iwamoto, J. Am. Ceram. Soc. **84**, 2213 (2001).
[14] J. F. Justo, F. de Brito Mota, and A. Fazzio, Phys. Rev. B **65**, 073202 (2002).
[15] R. K. Kalia, A. Nakano, A. Omeltchenko, K. Tsuruta, and P. Vashishta, Phys. Rev. Lett. **78**, 2144 (1997).
[16] R. K. Kalia, A. Nakano, K. Tsuruta, and P. Vashishta, Phys. Rev. Lett. **78**, 689 (1997).
[17] K. Tsuruta, A. Omeltchenko, R. K. Kalia, and P. Vashishta, Europhys. Lett. **33**, 441 (1996).
[18] K. Tsuruta, A. Nakano, R. K. Kalia, and P. Vashishta, J. Am. Ceram. Soc. **81**, 433 (1998).
[19] P. Ordejón and F. Ynduráin, J. Non-Cryst. Solids **137-138**, 891 (1991).
[20] F. Alvarez and A. A. Valladares, Solid State Commun. **127**, 483 (2003).
[21] F. Alvarez and A. A. Valladares, Phys. Rev. B **68**, 205203 (2003).
[22] L. Giacomazzi and P. Umari, Phys. Rev. B **80**, 144201 (2009).
[23] F. Wooten, K. Winer, and D. Weaire, Phys. Rev. Lett. **54**, 1392 (1985).

[24] P. Kroll, J. Non-Cryst. Solids **293-295**, 238 (2001).
[25] S. Z. Karazhanov, P. Kroll, A. Holt, A. Bentzen, and A. Ulyashin, J. Appl. Phys. **106**, 053717 (2009).
[26] I. Štich, R. Car, and M. Parrinello, Phys. Rev. Lett. **63**, 2240 (1989).
[27] L. Ouyang and W. Y. Ching, Phys. Rev. B **54**, R15594 (1996).
[28] F. de Brito Mota, J. F. Justo, and A. Fazzio, J. Appl. Phys. **86**, 1843 (1999).
[29] K. Jarolimek, R. A. de Groot, G. A. de Wijs, and M. Zeman, Phys. Rev. B **79**, 155206 (2009).
[30] K. Jarolimek, G. A. de Wijs, R. A. de Groot, and M. Zeman, Phys. Status Solidi A **207**, 605 (2010).
[31] J. P. Perdew, J. A. Chevary, S. H. Vosko, K. A. Jackson, M. R. Pederson, D. J. Singh, and C. Fiolhais, Phys. Rev. B **46**, 6671 (1992).
[32] G. Kresse and J. Hafner, Phys. Rev. B **47**, 558 (1993).
[33] G. Kresse and J. Furthmüller, Phys. Rev. B **54**, 11169 (1996).
[34] P. E. Blöchl, Phys. Rev. B **50**, 17953 (1994).
[35] G. Kresse and D. Joubert, Phys. Rev. B **59**, 1758 (1999).
[36] H. J. Monkhorst and J. D. Pack, Phys. Rev. B **13**, 5188 (1976).
[37] Under the assumption that H_2 molecules are not incorporated into the films during the deposition, the actual concentration of hydrogen in our cells would change. The low- and high-density cell would contain 24 at. % and 14 at. % of hydrogen, respectively. Expected changes in density are small due to the small hydrogen mass.
[38] M. Yashima, Y. Ando, and Y. Tabira, J. Phys. Chem. B **111**, 3609 (2007).
[39] N. Ashcroft and D. Langreth, Phys. Rev. **156**, 685 (1967).
[40] A. Bhatia and D. Thornton, Phys. Rev. B **2**, 3004 (1970).
[41] Neutron scattering lengths and cross sections, http://www.ncnr.nist.gov/resources/n-lengths/
[42] M. Misawa, T. Fukunaga, K. Niihara, T. Hirai, and K. Suzuki, J. Non-Cryst. Solids **34**, 313 (1979).
[43] E. A. Davis, N. Piggins, and S. C. Bayliss, J. Phys. C **20**, 4415 (1987).